Electronic Supplementary Information

Pressure-Induced White-Light Emission of a Cu(I) Cluster with Effective Blue Phosphorescence

Xin-Yi Wu,[a] Ji-Tong Xu,[a] Dan-Qing Liu,[a] Bei-Qi Ou,[a] Hui-Ying Zhang,[a] Chen-Hui Li,[a] Jia-Wen Ye*,[a] Ling Chen*,[a] Xiao-Ming Chen.[b]

[a]Jiangmen Key Laboratory of Synthetic Chemistry and Cleaner Production, School of Environmental and Chemical Engineering, Wuyi University, Jiangmen, Guangdong 529000, PR China

[b]MOE Key Laboratory of Bioinorganic and Synthetic Chemistry, School of Chemistry, IGCME, Sun Yat-Sen University, Guangzhou 510275, PR China.

Experiments and Method

Methods and Materials. All commercially available reagents and solvents were used as received without further purification. Powder X-ray diffraction (PXRD) patterns were recorded by a Rigaku Mini diffractometer. UV-Vis absorption spectra were recorded on a PerkinElmer Lambda950 UV-vis-NIR absorption spectrometer. Thermogravimetric (TG) analyses were performed by a Netzsch TG209F1 Libra R instrument with a ramping rate of 5.0 °C min^{-1} under nitrogen gas atmosphere. Elemental analyses (C, H, and N) were performed with an Elementar Vario EL elemental analyzer. Raman spectra were collected on LabRAM HR Evolution Raman spectrometer, excited at 633 nm. The Nicolet 6700 fourier transform infrared (FT-IR) spectrometer and KBr tablet were used to perform FT-IR spectra.

Single-Crystal X-ray Diffraction (SCXRD). Diffraction data were collected on a Rigaku XtaLAB single-crystal diffractometer equipped with micro focus sealed X-ray tube (Cu Kα, λ = 1.54178 Å) and PILATUS 200K detector at 150 and 300 K, respectively. The structures of **1** were solved with the direct methods and refined with the full-matrix least-squares method on F^2 using the SHELXTL package. Anisotropic thermal parameters were used to refine all non-hydrogen atoms. Hydrogen atoms were generated geometrically. Additional crystallographic information is available in the Table S1. CCDC 2354626 and 2354627 contain the supplementary crystallographic data for this paper. These data can be obtained free of charge from the Cambridge Crystallographic Data Centre via www.ccdc.cam.ac.uk/data_request/cif.

Photoluminescence Measurement. The emission spectra were recorded by Edinburgh FLS1000 fluorescence spectrometer equipped with a continuous Xe lamp. All instrument parameters such as the excitation split, emission split, and scanning speed were fixed during the in-situ measurements. Photoluminescence quantum yields (PLQYs) were performed by the same spectrometer in an integrating sphere (excited by 330 nm). The test temperature was controlled by an Oxford temperature controller. The fluorescence lifetime experiments were performed by the same spectrometer equipped with a flash Xe lamp and a VPL at 375±10 nm as the excitation sources. The pressure-dependent emission spectra were performed with a diamond-

anvil cell (DAC, High-Pressure Diamond Optics).

Density Functional Theory (DFT) Calculations. DFT calculations were performed using Gaussian 09 program.[1] Geometry optimizations were performed using by PBE0 density function with D3 dispersion correction.[2] The 6-31G(d) basis set were used for C, N and H, while LanL2DZ pseudopotentials were used for P, Cu and I. The unrestricted DFT calculations were employed to optimize the T_1 structure with the same function and basis set.

Time-Dependent Density Functional Theory (TDDFT) Calculations. TDDFT calculations were used to investigate the photophysical properties of the compounds. The calculations were performed with the same function and basis set as described for the DFT optimizations. The first 15 singlet states without geometry optimization were calculated for the transition of $S_1 \rightarrow S_0$. The first 5 triplet states without geometry optimization were calculated for the transition of $T_1 \rightarrow S_0$ based on the T_1 structure, which is optimized by the unrestricted DFT calculation. The Milliken orbital composition analyses were calculated by the Multiwfn program.[3]

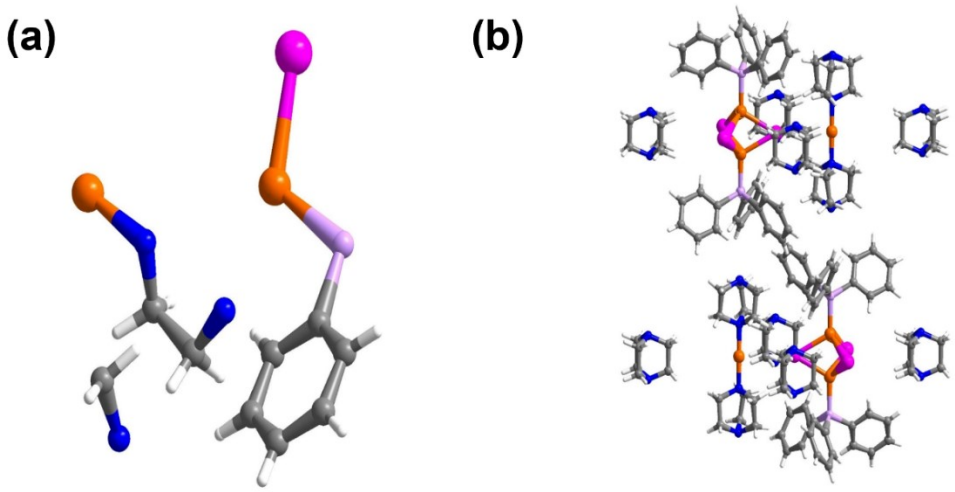

Figure S1. (a) The asymmetric unit and (b) the crystal stacking diagram of **1**. Colour codes for (a, b): C, grey; H, white; N, blue; Cu, orange; I, pink; P, lavender.

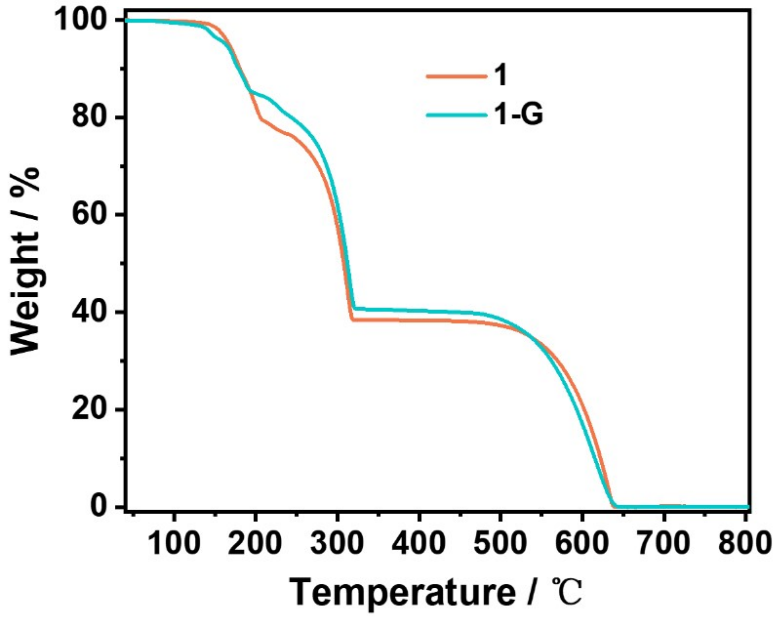

Figure S2. TG curves of **1** and **1-G**.

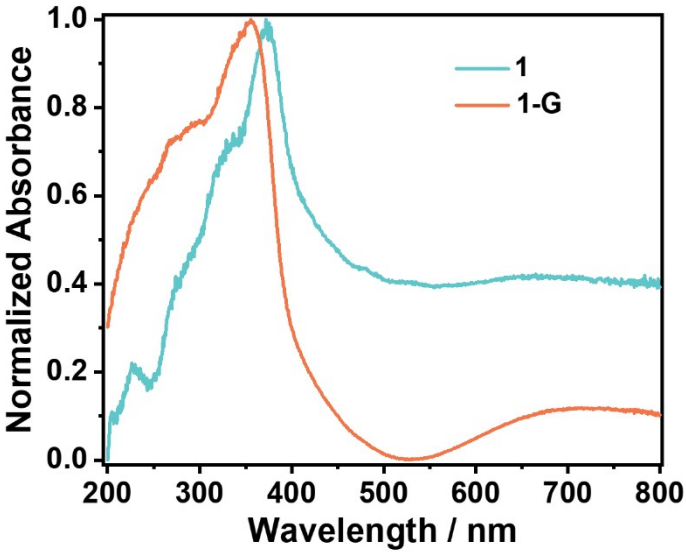

Figure S3. UV-Vis absorption spectra of **1** and **1-G**.

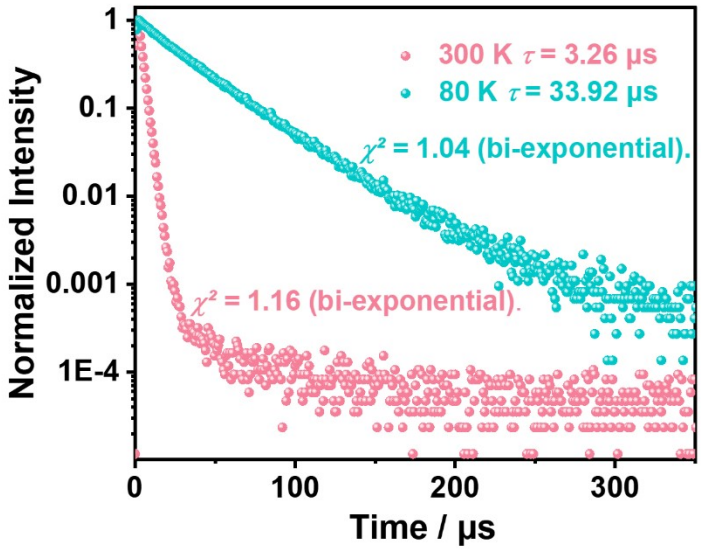

Figure S4. The decay profiles of **1** at 80 K, 300 K, excited by 375-nm VPL and detected at λ_{em}.

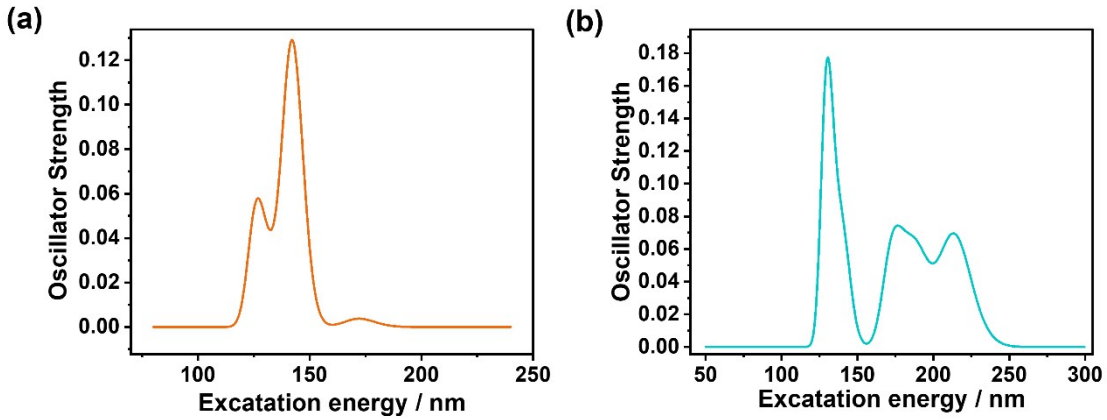

Figure S5. The simulated absorption spectra of (a) $[Cu(DABCO)_2]^+$ and (b) DABCO, evaluated by TDDFT calculations.

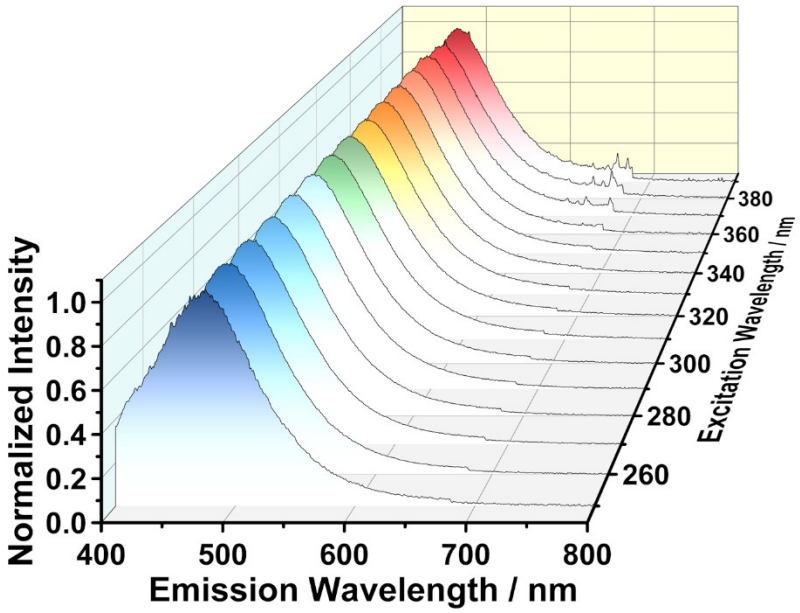

Figure S6. The excitation-emission map of **1** at room temperature.

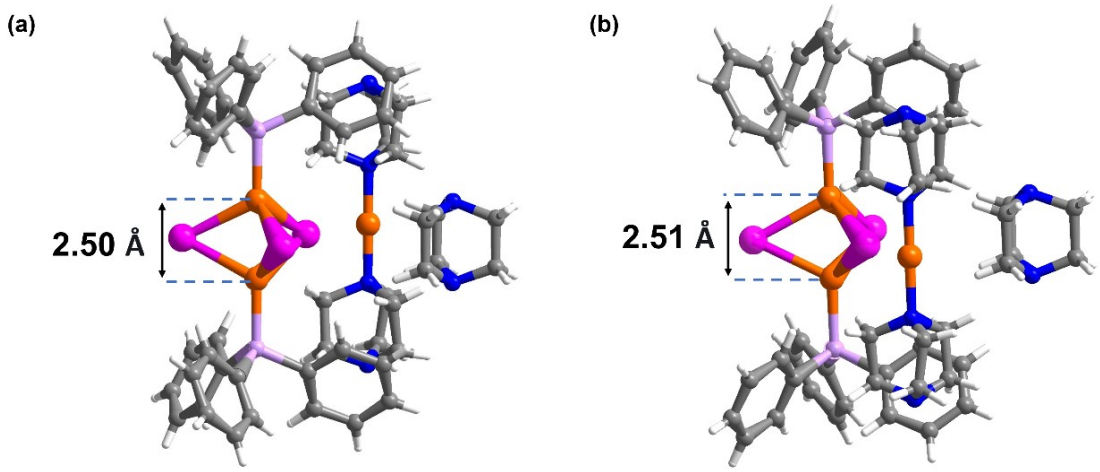

Figure S7. The Cu···Cu distances of **1** at (a) 150 K and (b) 300 K. Colour codes for (a, b): C, grey; H, white; N, blue; Cu, orange; I, pink; P, lavender.

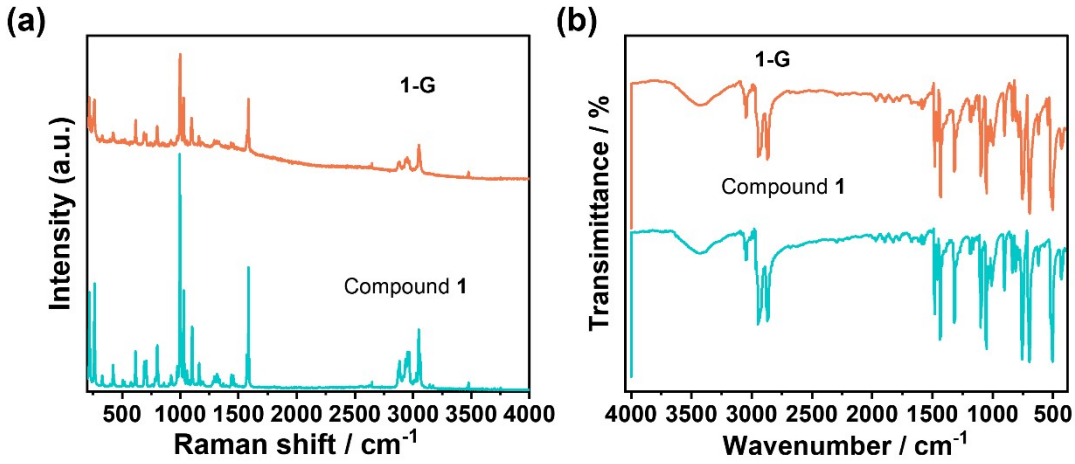

Figure S8. (a) The Raman and (b) FT-IR spectra of **1** before and after grinding.

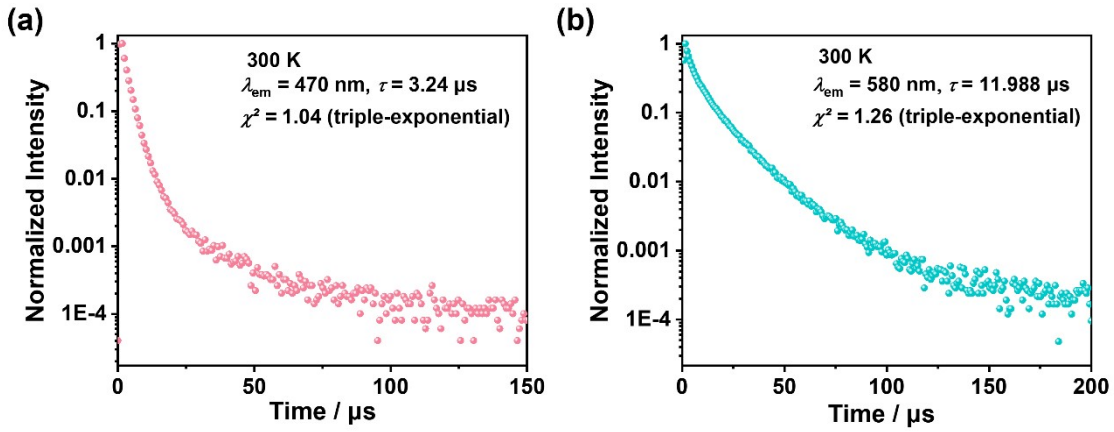

Figure S9. The decay profiles of **1-G**, detected at (a) 470 nm and (b) 580 nm and excited by 375-nm VPL.

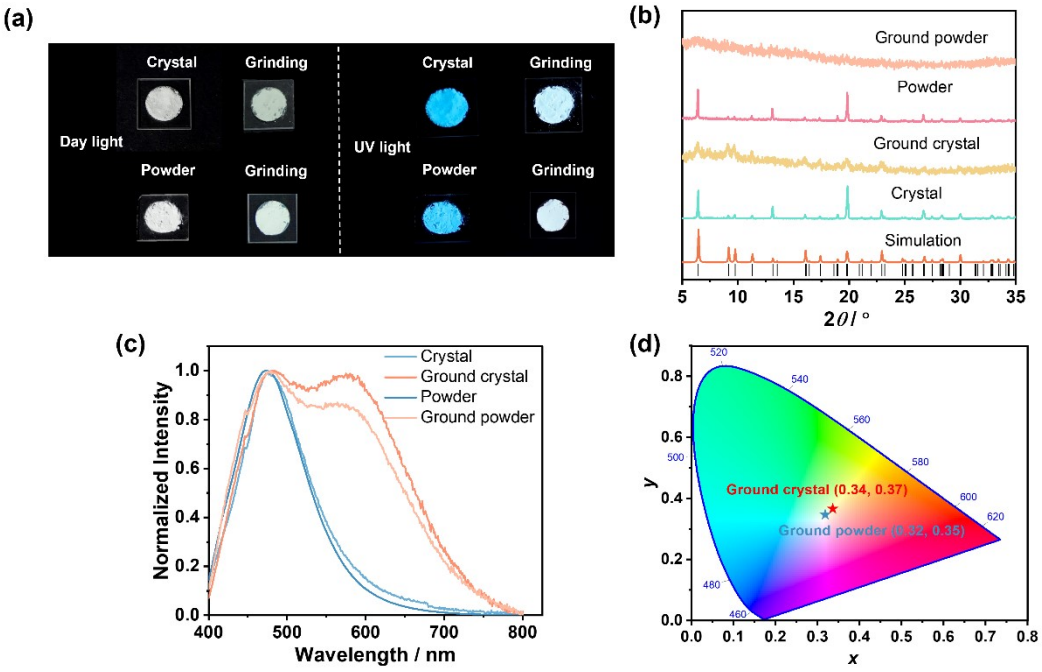

Figure S10. (a) Photographs of **1** crystal and powder before and after grinding, under day light and 365 nm UV light, respectively. (b) PXRD patterns of **1** crystal and powder before and after grinding, respectively. (c) Emission spectra of **1** crystal and powder before and after grinding, respectively, excited at 365 nm. (d) Commission Internationale de L'Eclairage (CIE) coordinates of **1** crystal and powder after grinding, based on (c).

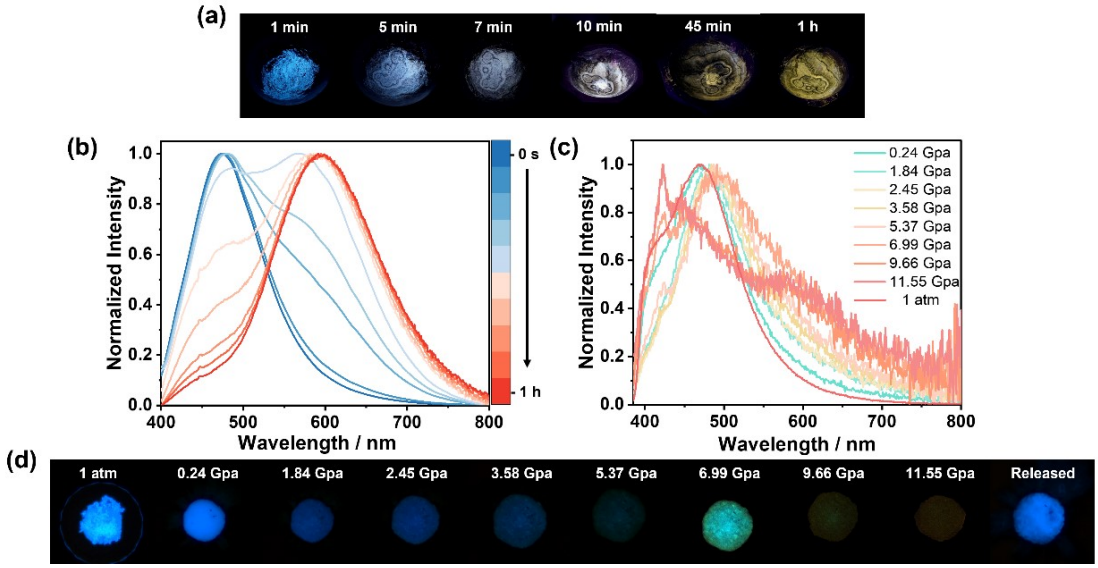

Figure S11. (a) Photographs and (b) emission spectra of **1** after grinding for different times, respectively, under 365 nm UV light. (c) Pressure-dependent emission spectra and (d) photographs of **1**, respectively, under 365 nm UV light.

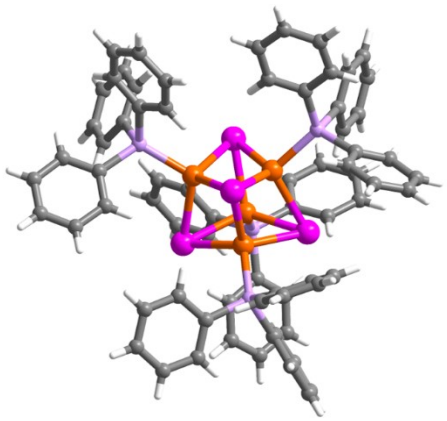

Figure S12. Structures of $[Cu_4I_4(TPP)_4]$. Colour codes: C, grey; H, white; Cu, orange; I, pink; P, lavender

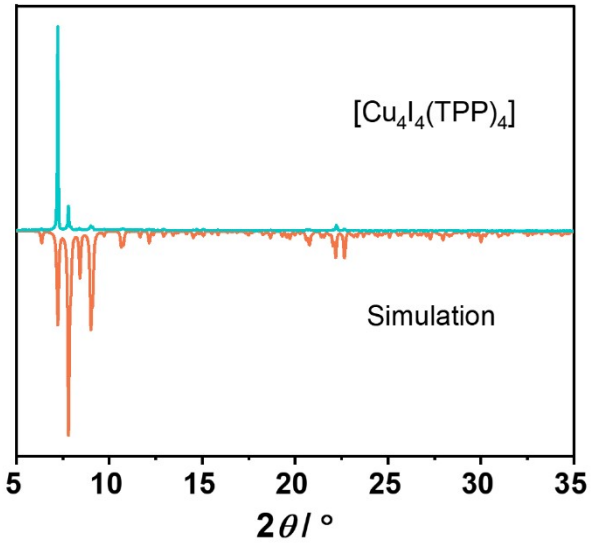

Figure S13. PXRD pattern of $[Cu_4I_4(TPP)_4]$.

Table S1. Crystallographic data and structural refinement detail of **1**.

Complex	300 K	150 K
Formula	$C_{54}H_{66}Cu_3I_3N_6P_2$	$C_{54}H_{66}Cu_3I_3N_6P_2$
Formula weight	1432.38	1432.38
Temperature / K	298.49(10)	149.99(10)
Crystal system	hexagonal	hexagonal
Space group	$P6_3/m$	$P6_3/m$
a / Å	10.8743(2)	10.7977(2)
b / Å	10.8743(2)	10.7977(2)
c / Å	26.5205(4)	26.3492(4)
α / °	90	90
β / °	90	90
γ / °	120	120
Volume / Å^3	2715.91(11)	2660.48(11)
Z	2	2
R_{int}	0.0476	0.0459
$R_1[I > 2\sigma(I)]$[a]	0.0429	0.0372
$wR_2[I > 2\sigma(I)]$[b]	0.1063	0.0889
R_1 (all data)	0.0459	0.0400
wR_2 (all data)	0.1083	0.0903
GOF	1.089	1.065

[a] $R_1 = \Sigma||F_o| - |F_c||/\Sigma|F_o|$

[b] $wR_2 = [w(F_o^2 - F_c^2)^2/\Sigma w(F_o^2)^2]^{1/2}$

Table S2. The energy gap, λ_{em} and composition in terms of main orbital transitions of $[Cu_2I_3(TPP)_2]^-$ calculated by TDDFT and the Multiwfn program.

Energy Gap (eV)	λ_{em} (nm)	Charge transfer of the transition(M/XLCT)
2.81	440	H→L (95.66%)

Table S3. The CIE, CCT and CRI / R_a of reported Cu(I) coordination compounds.

Compound	CIE	CCT (K)	CRI / R_a	Ref.
This work	(0.30, 0.35)	6856	81.5	-
$[(C_{12}H_{24}O_6)CsCu_2Br_3]$[a]	(0.34, 0.43)	4962	73.7	*J. Phys. Chem. Lett*. 2021, **12**, 12345−12351
$[Na_4$(18-crown-6)$_5In_2Cu_4Br_{14}\cdot 8H_2O]$[a]	(0.37, 0.42)	4429	75	*Adv. Opt. Mater*. 2022, **10**, 2200944
[(18-crown-6)$_2Na_2(H_2O)_3Cu_4I_6$ (CNCl) + KSF: Mn^{4+}] [b]	(0.32, 0.34)	5859	89.6	*Chem. Mater*. 2021, **33**, 4382−4389
[0D-Cu_2I_2(tpp)$_2$(3-pc)$_2$ + 1D-Cu_2I_2(tpp)$_2$(2,5-dm-pz)][b]	(0.30, 0.36)	8001	63.6	*J. Mater. Chem. C*, 2017,**5**, 5962-5969
[1D-Cu_2I_2(tpp)$_2$(bpp) + 1D-Cu_2I_2(tpp)$_2$(4,4'-bpy)][b]	(0.31, 0.36)	4512	73,8	*Adv. Funct. Mater*. 2018, **28**, 170559
[$(C_{20}H_{20}P)_2Cu_2I_4$ + $BaMgAl_{10}O_{17}:Eu^{2+}$(4.7%)] [b]	(0.31, 0.37)	6573	78	*Inorg. Chem*. 2023, **62**, 18825−18829

[a]The WLED based on single-component white light emitters. [b]The WLED based on multi-component phosphors.

References

[1] M. J. Frisch, G. W. Trucks, H. B. Schlegel, G. E. Scuseria, M. A. Robb, J. R. Cheeseman, G. Scalmani, V. Barone, B. Mennucci, G. A. Petersson, H. Nakatsuji, M. Caricato, X. Li, H. P. Hratchian, A. F. Izmaylov, J. Bloino, G. Zheng, J. L. Sonnenberg, M. Hada, M. Ehara, K. Toyota, R. Fukuda, J. Hasegawa, M. Ishida, T. Nakajima, Y. Honda, O. Kitao, H. Nakai, T. Vreven, Jr J. A. Montgomery, J. E. Peralta, F. Ogliaro, M. Bearpark, J. J. Heyd, E. Brothers, K. N. Kudin, V. N. Staroverov, R. Kobayashi, J. Normand, K. Raghavachari, A. Rendell, J. C. Burant, S. S. Iyengar, J. Tomasi, M. Cossi, N. Rega, J. M. Millam, M. Klene, J. E. Knox, J. B. Cross, V. Bakken, C. Adamo, J. Jaramillo, R. Gomperts, R. E. Stratmann, O. Yazyev, A. J. Austin, R. Cammi, C. Pomelli, J. W. Ochterski, R. L. Martin, K. Morokuma, V. G. Zakrzewski, G. A. Voth, P. Salvador, J. J. Dannenberg, S. Dapprich, A. D. Daniels, O. Farkas, J. B. Foresman, J. V. Ortiz, J. Cioslowski, D. J. Fox. *Gaussian, Inc.*, Wallingford CT, 2009.

[2] C. Adamo, V. Barone, Toward reliable density functional methods without adjustable parameters: The PBE0 model. *J. Chem. Phys.* 1999, **110**, 6158.

[3] T. Lu, F. Chen, *J. Comput. Chem*. 2012, **33**, 580.